J Fluoresc (2013) 23:963–974
DOI 10.1007/s10895-013-1222-x

ORIGINAL PAPER

Fluorescence "Switch on" of Conjugates of CdTe@ZnS Quantum Dots with Al, Ni and Zn Tetraamino-Phthalocyanines by Hydrogen Peroxide: Characterization and Applications as Luminescent Nanosensors

Oluwasesan Adegoke · Samson Khene · Tebello Nyokong

Received: 8 February 2013 / Accepted: 1 April 2013 / Published online: 20 April 2013

Abstract In this study, we have developed a novel nanoprobe for H_2O_2 based on the conjugation of CdTe@ZnS quantum dots (QDs) to different metal tetraamino-phthalocyanine (MTAPc): (M=(OAc)Al, {OAc=acetate}, Ni and Zn). Chemical coordination of the QDs to the MTAPc resulted in the fluorescence "switch off" of the linked QDs which was associated with Förster resonance energy transfer (FRET). In the presence of varying concentration of H_2O_2, the fluorescence of the linked QDs was progressively "switched on" and the FRET mechanism between the QDs and the MTAPc was disrupted. The sensitivity/limit of detection of the nanoprobe followed the order: QDs-ZnTAPc (2.2 μM)>QDs-NiTAPc (4.4 μM)>QDs-AlTAPc (9.8 μM) while the selectivity followed the order: QDs-NiTAPc>QDs-AlTAPc>QDs-ZnTAPc. The varying degree of sensitivity/selectivity and mechanism of detection is discussed in detail.

Keywords Quantum dots · Phthalocyanine · Hydrogen peroxide · Resonance energy transfer

Introduction

Exploring the use of nanoassemblies, which incorporates the use of semiconductor nanocrystal quantum dots (QDs) as fluorescence probes, has drawn considerable attention over the past decade [1–8]. The optical properties of QDs, makes them unique nanomaterials for optical sensor technology. Also, the luminescence properties of QDs are determined by physical or chemical interactions taking place at the surface. Such interactions may lead to either fluorescence quenching or enhancement [1, 9].

To date, different surface modification strategies have been employed in stabilizing the luminescence state of QDs. Macrocyclic compounds such as calixarenes [10], cyclodextrins [11] crown ether [12] and porphyrins [13] have been used for stabilizing the QDs, and the resulting host-molecule complexes employed for molecular recognition of ions and small molecules.

In order to explore novel strategies for surface modification of QDs for tailored sensor development with improved sensitivity and selectivity, we report here on the conjugation of thiol-capped CdTe@ZnS QDs to another class of macrocylic compound known as phthalocyanines (Pcs). Pcs and their metallophthalocyanine derivatives (MPcs) are two-dimensional 18 π-electron aromatic porphyrin synthetic analogues [14]. They have attracted a lot of interest in recent years not only for their applications as dye and pigments, but also as chemical sensors [15]. They are also known to be non-toxic. Amino substituted Pcs have been chemically linked to QDs and the Förster resonance energy transfer (FRET) behaviour studied [16–20]. Electrochemical behaviour of QDs linked to nickel phthalocyanines has also been studied [21]. To date, nothing is known about the coupling of MPc to QDs for optical sensing. To this end, we have developed a novel strategy for the surface modification of QDs by covalent linking of (OAc)Al (OAc=acetate), Ni and Zn tetraamino-phthalocyanine (TAPc) to 3-mercaptopropionic acid (MPA)-capped CdTe@ZnS QDs and investigated the nanoconjugate for its ability to selectively detect hydrogen peroxide (H_2O_2) in aqueous solution as a test molecule.

O. Adegoke · S. Khene · T. Nyokong (✉)
Department of Chemistry, Rhodes University,
Grahamstown 6140, South Africa
e-mail: t.nyokong@ru.ac.za

H_2O_2 is a reactive oxygen specie (ROS) and a by-product of many metabolic reactions. There is a need to detect H_2O_2 because excessive production beyond the physiological range often leads to oxidative stress. Among the different central metals used in this work, only AlTAPc has been reported for fluorescence sensing of H_2O_2, but in the absence of QDs [22, 23]. The efficiency of sensing of H_2O_2 using QDs linked to (OAc)AlTAPc is compared to that of NiTAPc and ZnTAPc. It is possible that the coupling of MTAPc to the QDs can influence the efficacy of sensitivity and selectivity of the nanoprobe towards H_2O_2. The mechanism of detection is studied based on the fluorescence "off/on" mode.

Experimental

Materials

1-Ethyl-3-(3-dimethylaminopropyl)-carbodiimide (EDC), N-hydroxysuccinimide (NHS), L-glutathione, L-cysteine, cysteamine, $CdCl_2.2.5.H_2O$, t-butyl hydroperoxide (TBHP), sodium borohydride, thioglycolic acid (TGA) and 3-mercaptopropionic acid (MPA) were obtained from Sigma-Aldrich. Absolute ethanol, Na_2HPO_4, $(NH)_2Fe(SO_4)_2.7H_2O$, KCl, HCl, H_2O_2, NaCl, $NaNO_2$, $NaNO_3$, zinc powder, KOH and dimethylformamide (DMF) were obtained from SAARCHEM. $NaClO_4.H_2O$ and urea was obtained from BDH chemicals. All solutions were prepared with ultra pure water obtained from a Milli-Q Water System (Millipore Corp. Bedford, MA, USA). All measurements for the detection of H_2O_2 were carried out in physiological condition using 50 mM PBS pH 7.4. The pH of the buffer solution was adjusted by addition of 1.0 M NaOH or HCl. Metal-free (H_2)TAPc, (OAc)AlTAPc, NiTAPc and ZnTAPc were synthesized according to previously reported procedures for other TAPc [24].

Instrumentation

Excitation and emission spectra were recorded on a Varian Eclipse spectrofluorimeter. Ground state electronic absorption spectra were recorded on a Shimadzu UV–vis 2550 spectrophotometer. X-ray powder diffraction patterns were recorded using a Cu kα radiation (λ=1.5405 Å, nickel filter), on a Bruker D8 Discover equipped with a proportional counter. A Metrohm Swiss 827 pH meter was used for pH measurements. FT-IR spectra were obtained on a Perkin-Elmer spectrum 100 with universal attenuated total reflectance (ATR) sampling accessory. Transmission electron microscopy (TEM) images were obtained using a Zeiss Libra TEM 120 model operated at 90 kV. Gaussian 03 program using an Intel/Linux cluster was used for density functional theorem (DFT) calculations [25]. Fluorescence lifetime measurements were carried out using a time-correlated single photon counting (TCSPC) setup (FluoTime 200, Picoquant GmbH). The excitation source was a diode laser (LDH-P-C-485 with 10 MHz repetition rate, 88 ps pulse width and wavelength of 480 nm).

Synthesis of MPA-CdTe@ZnS QDs (Scheme 1)

CdTe@ZnS QDs capped with MPA was prepared from core TGA-capped CdTe QDs by following the methods described in literature with slight modifications [26, 27]. Firstly, TGA-capped CdTe QD was synthesized following literature procedures [26]. The mole ratio of Cd:Te:TGA used was 1:2.3:3.0. After 30 min of core CdTe growth, a 40 ml aqueous solution (pH=8) containing MPA (4 mmol) and $ZnCl_2$ (2 mmol, 0.27 g) was added into the core QDs solutions to obtain MPA-CdTe@ZnS QDs. MPA was used as both the capping ligand and sulphur source for the growth of the core-shell QDs. Using this procedure, it is expected that the MPA ligand is exchanged with TGA in the core-shell solution [28]. The solution was heated to 100 °C with

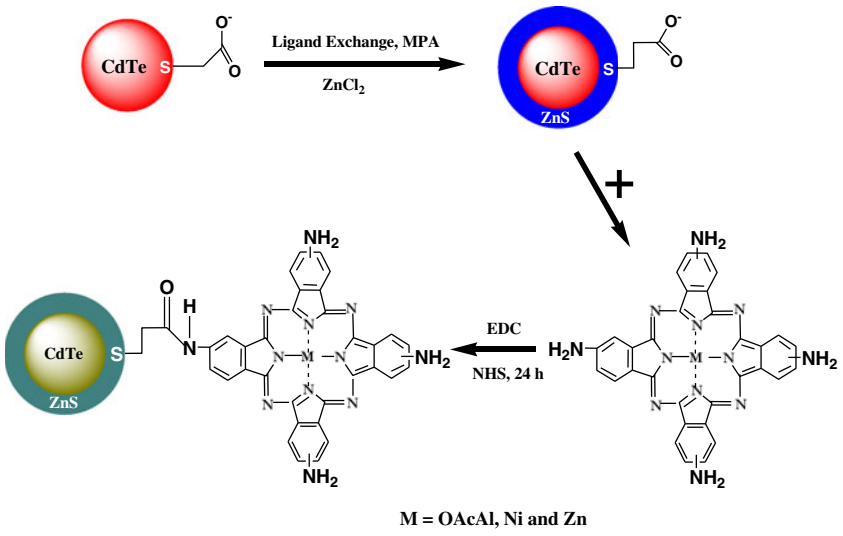

Scheme 1 Schematic representation showing the preparation of QDs and QDs-MTAPc nanoconjugate

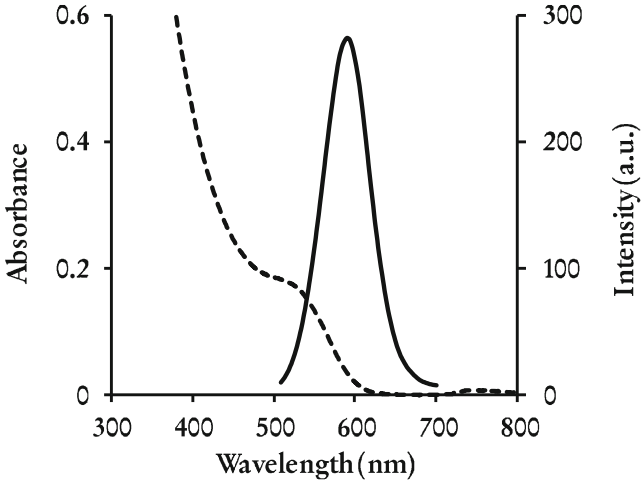

Fig. 1 Fluorescence (*solid line*) and absorption (*dashed line*) spectra of QDs before conjugation. Solvent: 50 mM PBS pH 7.4, λ_{exc}=490 nm

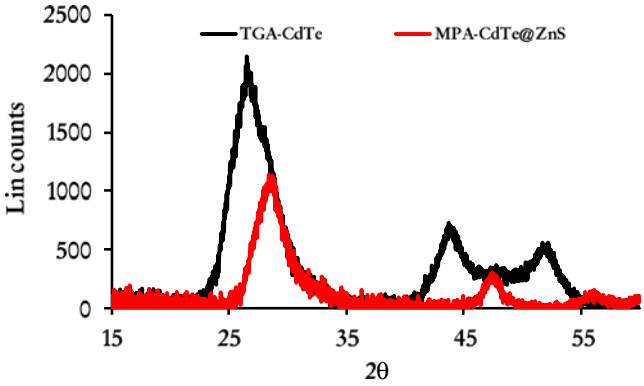

Fig. 2 Powder XRD spectra of TGA-CdTe and MPA-CdTe@ZnS QDs

time to control the sizes of the core-shell QDs. Aliquots of each reaction mixture were taken at different time intervals for emission and absorption measurements. The core-shell QDs (MPA-CdTe@ZnS) were precipitated out with ethanol, centrifuged, dried under vacuum and kept in the dark for further use.

Conjugation of QDs to MTAPc (Scheme 1)

The strategy employed in this work was based on standard procedure described previously in literature for coupling MPcs to QDs via an amide bond [20, 21] but with some slight modification. Briefly, to a solution of 10 mg MPA-CdTe@ZnS in 50 mM PBS pH 7.4 was added 0.1 M EDC (in water) to activate the carboxylate group of the QDs. The mixture was then stirred for 30 min at room temperature, after which a mixture of 0.1 M NHS (in water) and 2×10^{-6} M of H_2TAPc, (OAc)AlTAPc, NiTAPc or ZnTAPc in DMF:PBS pH 7.4 (3:2, *v*/*v*) was added and the stirring continued for 24 h. The resulting linked QDs-MTAPc complexes were precipitated out from solution by the addition of ethanol and centrifuged repeatedly to remove free QDs and also washed repeatedly with DMF to remove free MPc. The QDs-MPc colloid is not soluble in the two solvents. The obtained QDs-MPc complexes were soluble in PBS buffer as a colloidal solution.

Table 1 Fluorescence quantum yields, FRET efficiency, quenching rate constant (K_a), and sensitivity values (K) for the QDs-MTAPc nanoprobe. Solvent: 50 mM PBS pH 7.4

Nanoconjugates	$^{a}\Phi_{F(QD)}^{conjugate}$	E_{ff}	$K_a(M^{-1})^{b}$	$K(M^{-1})$
QDs-AlTAPc	0.26	0.35	1.50×10^5	3.72×10^7
QDs-NiTAPc	0.10	0.69	7.24×10^5	8.25×10^7
QDs-ZnTAPc	0.09	0.71	2.21×10^5	1.67×10^8

[a] λ_{exc}=490 nm and Φ_F(QDs)=0.46

[b] Data determined from QDs mixed with MTAPc and not chemically linked

Procedures for the Optical Recognition of H_2O_2

Firstly, H_2O_2 solution was prepared by serial dilution of commercial 30 % stock solution. Separately, the QDs-MTAPc nanoconjugates were dissolved in 50 mM PBS pH 7.4 and ultrasonicated for 15 min to disperse the colloidal solution. Various concentrations of H_2O_2 were added to the QD-MTAPs solution. All the steps for fluorescence measurements with the ROS were performed sequentially. The interval between the measurements was 15 min in order to obtain a stable fluorescence signal for each concentration of H_2O_2. All measurements were recorded at room temperature.

Result and Discussion

Characterization of MPA-CdTe@ZnS QDs

The synthesis of MPA-CdTe@ZnS is depicted in Scheme 1. It is important to note that ZnS was used to passivate the surface of the core CdTe with the main aim of improving the optical properties of the core-shell QDs. Core-shell QDs are less toxic than core QDs [29]. Our group has reported that core-shell QDs show improved luminescence sensitivity and selectivity towards ROS than core QDs [30, 31]. Figure 1 shows the fluorescence emission and absorption spectra of the as-synthesized MPA-CdTe@ZnS QDs measured in 50 mM PBS pH 7.4. The QDs exhibit broad absorption and well-resolved emission spectra as expected. The emission and absorption maximum wavelength values for the QDs used in this work are: 590 nm and 514 nm, respectively, in 50 mM PBS pH 7.4.

The fluorescence quantum yield (Φ_F) of the QDs before conjugation was measured using the procedure reported in

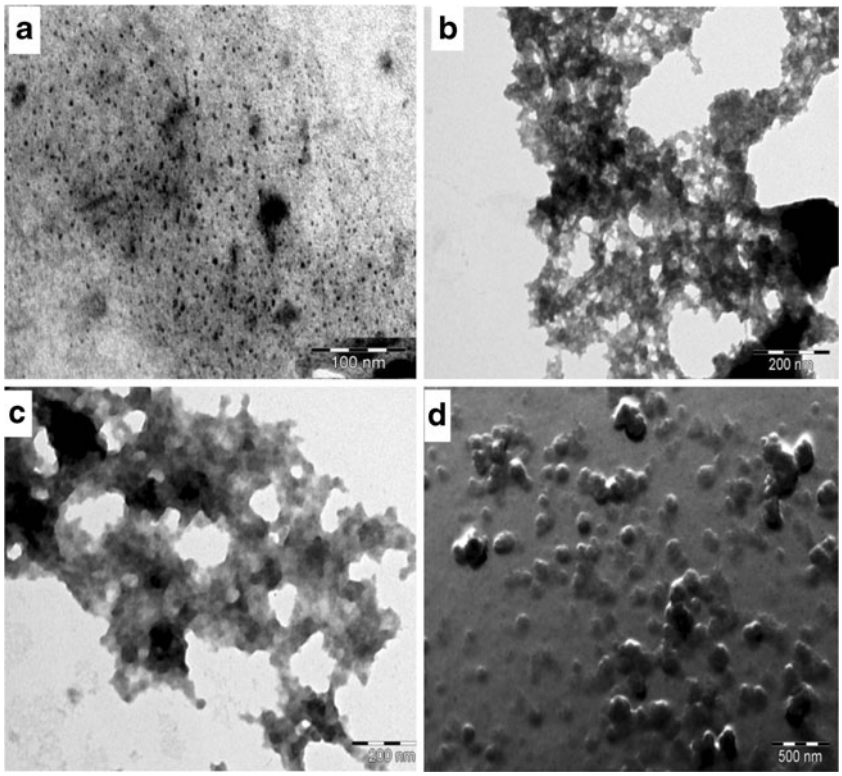

Fig. 3 TEM images of **a** CdTe@ZnS QDs, **b** QDs-AlTAPc, **c** QDs-NiTAPc and **d** QDs-ZnTAPc

literature [32], Eq. 1,

$$\Phi_F = \Phi_{F(Std)} \frac{F \cdot A_{Std} \cdot n^2}{F_{Std} \cdot A \cdot n_{Std}^2} \quad (1)$$

where A and A_{Std} are the absorbances of the sample and standard at the excitation wavelength, respectively. F and F_{Std} are the areas under the fluorescence curves of the QDs and the standard respectively and n and n_{Std} are the refractive indices of the solvent used for the sample and standard. Rhodamine 6G in ethanol (Φ_F=0.95 [32]) was used as the standard. The Φ_F value was 0.46 for MPA-CdTe@ZnS, Table 1.

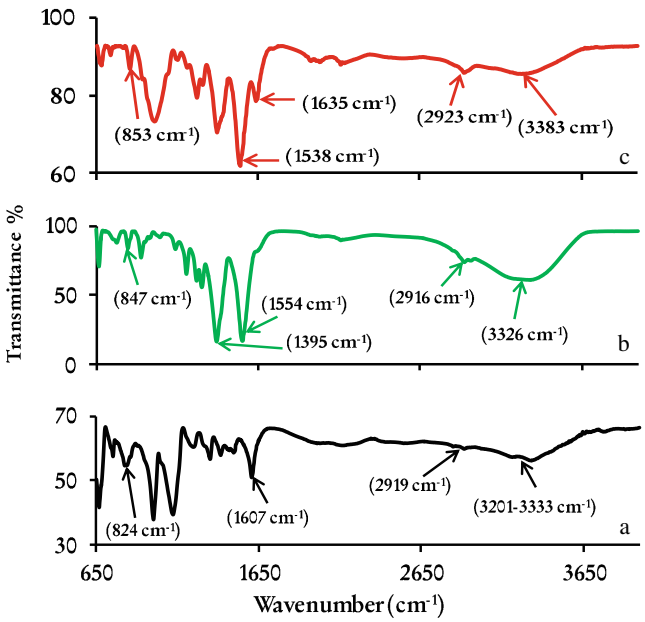

Fig. 4 FT-IR spectra of **a** (OAc)AlTAPc, **b** CdTe@ZnS QDs and **c** CdTe@ZnS-AlTAPc (used as a representative)

Shown in Fig. 2, are the powder XRD patterns of core CdTe and core-shell CdTe@ZnS. The diffraction pattern in Fig. 2 corresponds to planes at 110, 220 and 311, and displays three characteristic peaks for bulk CdTe having a zinc blend crystal structure and cubic ZnS structure for CdTe@ZnS QDs as previously reported in literature [33]. It can be seen from Fig. 2 that the 2θ values for TGA-CdTe QDs were at 26.6, 43.8 and 52.2° and those for MPA-CdTe@ZnS QDs were at 28.6, 47.4 and 56.2° respectively. It is commonly known that XRD peaks for the core QDs have lower 2θ values compared to core-shell QDs [34, 35]. The higher 2θ values of the CdTe@ZnS compared to CdTe QDs suggest that we have successfully formed the core-shell QDs. The size of the QDs was estimated using XRD, according to the Scherrer Eq. (2) [36].

$$d(\text{Å}) = \frac{k\lambda}{\beta \cos\theta} \quad (2)$$

where λ is the wavelength of the X-ray source (1.5405 Å), k is an empirical constant equal to 0.9, β is the full width at half maximum of the diffraction peak and θ is the angular position.

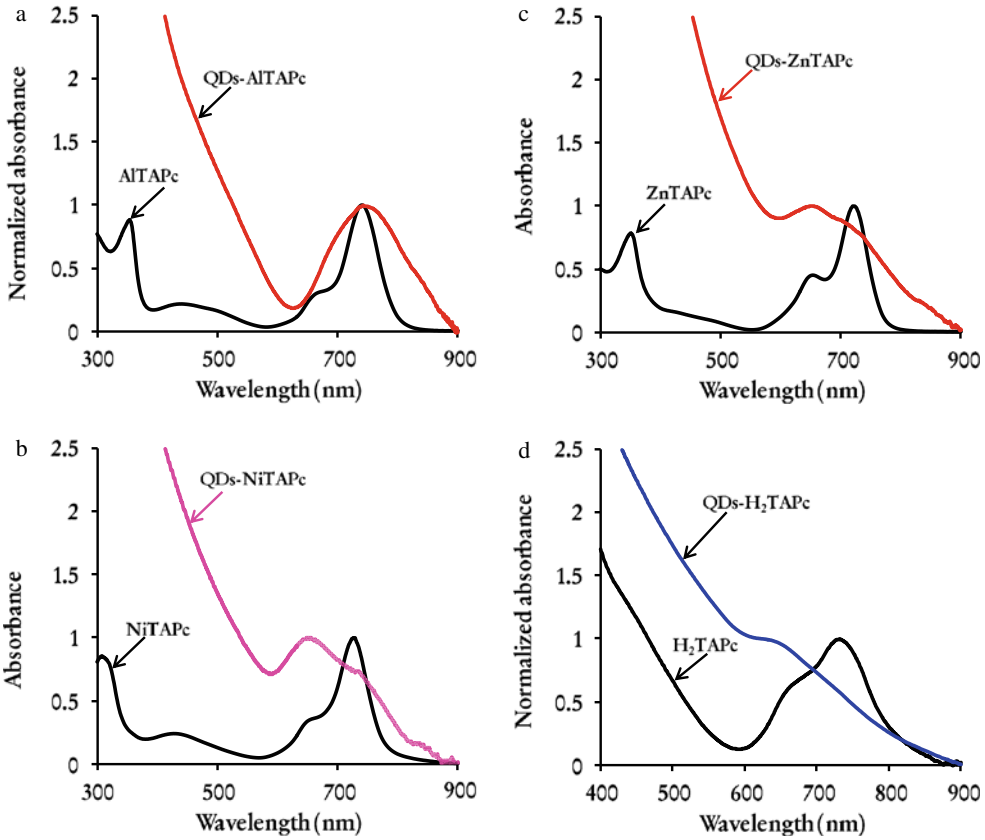

Fig. 5 Overlay of the UV/vis absorption spectra of **a** AlTAPc and QDs-AlTAPc, **b** NiTAPc and QDs-NiTAPc, **c** ZnTAPc and QDs-ZnTAPc and **d** H_2TAPc and QDs-H_2TAPc. Solvent for the Pc: DMF:PBS pH 7.4 (3:2, *v*/*v*) and solvent for the QDs-MTAPc: 50 mM PBS pH 7.4

The size obtained from XRD estimation is 3.0 nm for MPA-CdTe@ZnS.

Characterization of CdTe@ZnS QDs-MTAPc

It is possible that more than one MTAPc binds to one QDs. In fact, it has been determined that two ZnTAPc molecules bind to core QDs [19].

TEM Analysis

TEM was used to qualitatively study the morphology of the colloidal QDs before and after conjugation to the MTAPc (M=H_2, (OAc)Al, Zn and Ni) and also to determine the average size distribution of the QDs. The metal free H_2TAPc is not discussed in detail, since it did not show sensitivity towards hydrogen peroxide as discussed later in this work. Figure 3a shows that the CdTe@ZnS QDs alone are not aggregated but monodispersed and displayed individual particles with size ~3 nm. This size is similar to that obtained using XRD above. TEM images for the QDs-AlTAPc, QDs-NiTAPc and QDs-ZnTAPc are presented in Fig. 3b–d. It was observed that the QDs-AlTAPc and QDs-NiTAPc complexes displayed aggregation. For QDs-ZnTAPc, the shape of the complex is close to spherical but also relatively aggregated as with the rest of the complexes.

FT-IR and UV–Vis Spectral Characterization

Amide bonds were formed by linking the QDs to the MTAPcs and FT-IR was employed to confirm the formation of such bond. Figure 4 shows the FT-IR spectra of (OAc)AlTAPc, QDs and QDs-AlTAPc. (OAc)AlTAPc is used as a representative for the rest of the MTAPc since the spectra were similar to each other. For (OAc)AlTAPc alone, the partially split band around 3,201–3,333 cm^{-1} originates from the symmetric and asymmetric N–H stretching mode of the primary amine group and this is supported by the presence of the corresponding N–H bending mode at 1,607 cm^{-1} [24]. Also, the C–H bending and stretching modes are found at 824 and 2,919 cm^{-1} respectively. For the QDs, the symmetric and asymmetric COO^- stretching band were observed at 1,395 and 1,554 cm^{-1}. The corresponding –OH band is found at 3,326 cm^{-1} and the C–H bending and stretching mode are found at 847 and 2,916 cm^{-1}. For the QDs-AlTAPc spectrum, the formation of bands corresponding to 1,635 cm^{-1} (primary amide I) and 1,538 cm^{-1} (secondary amide II) are observed as a strong indication for the successful conjugation of the QDs-MTAPc [37, 38].

The ground-state electronic absorption spectra of the MTAPcs and QDs-MTAPc are overlayed in Fig. 5a–d. It is evident that the Q band position of these MTAPcs: (OAc)AlTAPc (741 nm), NiTAPc (727 nm), ZnTAPc

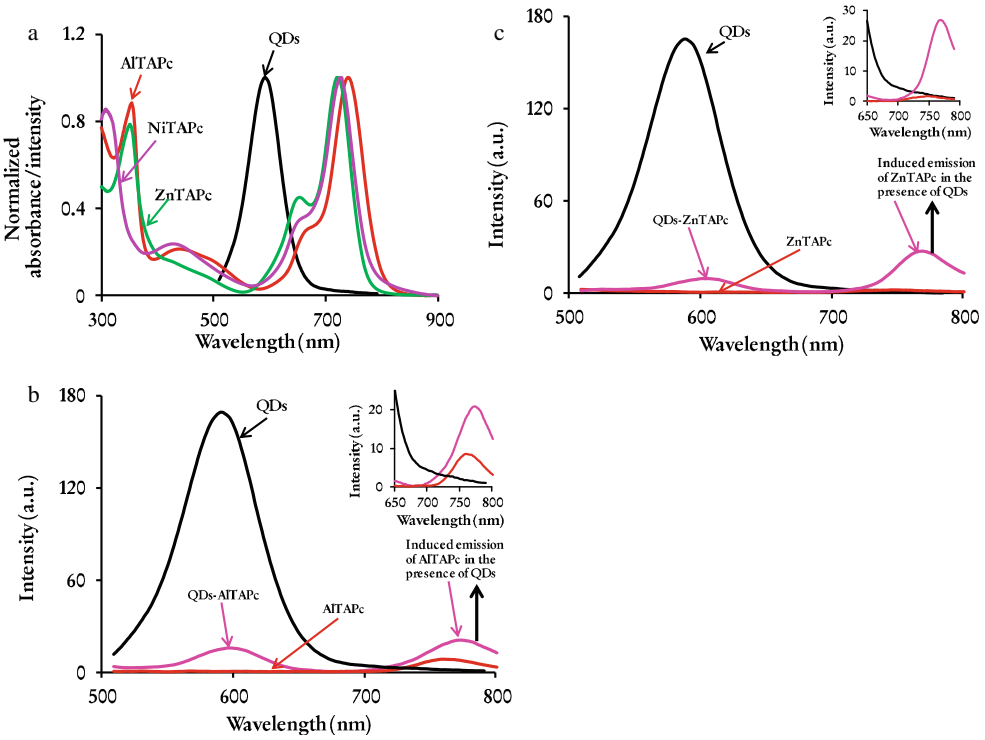

Fig. 6 (**a**) Normalized intensity/absorbance showing the overlap between the QDs and MTAPc (M = Al, Ni and Zn). Induced emission of AlTAPc (**b**) and ZnTAPc (**c**) through energy transfer from the QDs in the conjugate. Insets: Expanded view for induced emission. λ_{exc}=490 nm

(721 nm) and H_2TAPc (732 nm) are all red shifted in DMF:PBS solvent mixture compared to unsubstituted derivatives of 670 nm (ZnPc). The red shifting is typical of MTAPc, due to the electron donating nature of the NH_2 substituents [24]. The solvent mixture of DMF:PBS (3:2) was employed for MTAPc complexes in order to ensure the presence of aqueous environment used for the conjugate. The MTAPc complexes are not soluble in aqueous media. For the QDs-MTAPc complexes (Fig 5a–d) measured in 50 mM PBS pH 7.4 buffer, the absorption spectra show a significant change from the MTAPc alone. The absorption spectra of the linked MTAPcs are broadened and in some cases, additional blue shifted bands are observed. Both the broadening and blue shifted bands are associated with aggregation. It is important to note that the spectra of the conjugates were obtained from the colloidal suspension which would also result in aggregation.

Fluorescence Quenching

It is well known that the fluorescence of QDs is due to the recombination of electron–hole pair upon excitation, and suppression of the radiative recombination process results in fluorescence quenching [3]. Quenching of QDs emission by Pc is expected through Förster resonance energy transfer (FRET) [3, 39]. For FRET to occur, there has to be an overlap between the emission spectrum of the donor (QDs) and the absorption spectrum of the acceptor (MTAPc) as observed in Fig. 6a. In the absence of the QDs, there was a very weak fluorescence for (OAc)AlTAPc (Fig. 6b) and ZnTAPc (Fig. 6c) complexes on excitation at 490 nm. This indicates that the stimulated emission of the AlTAPc (Fig. 6b) and ZnTAPc (Fig. 6c) that emerged in the conjugate is due to the induced non-radiative energy transfer from the QDs to the MTAPcs. NiTAPc is non-fluorescent due to the open-shell nature of the central metal. However FRET efficiency was determined from the photoluminescence decrease of the donor for NiTAPc. For ZnTAPc and AlTAPc, both stimulated emission and decrease in CdTe@ZnS

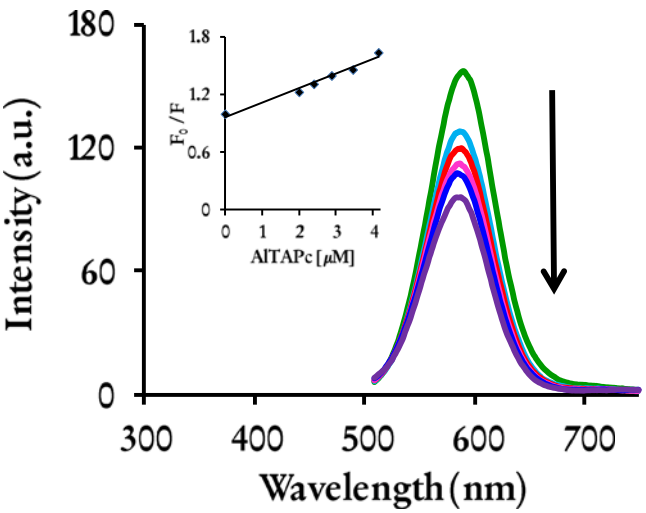

Fig. 7 Fluorescence quenching spectra of the QDs in the presence of increasing concentration of AlTAPc. [AlTAPc]=0–4.15×10^{-6} M. Inset: corresponding Stern-Volmer plot. λ_{exc}=490 nm

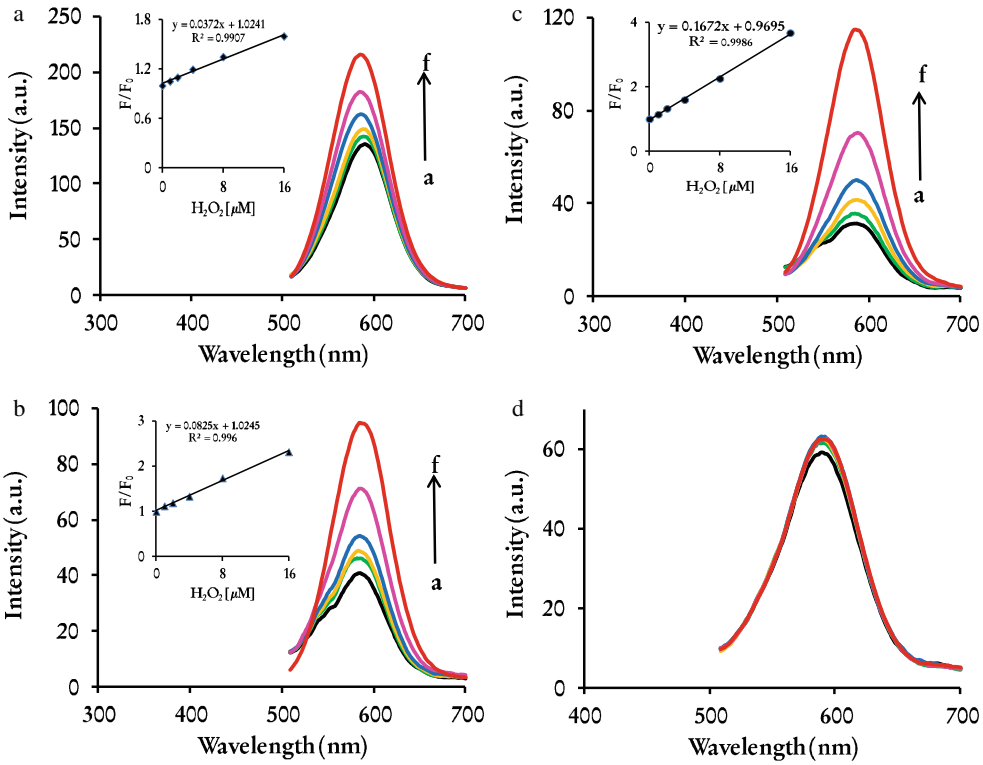

Fig. 8 Fluorescence emission spectra of **a** QDs-AlTAPc, **b** QDs-NiTAPc, **c** QDs-ZnTAPc and **d** QDs-H_2TAPc upon addition of varying concentration of H_2O_2. Inset: calibration curve of F/F_0 versus H_2O_2 concentration. [H_2O_2], *a–f*: 0, 1.0×10^{-9}, 2.0×10^{-9}, 4.0×10^{-9}, 8.0×10^{-9}, 1.6×10^{-8} M. λ_{exc}=490 nm

emission were used to quantify FRET efficiency. For comparative purposes, the values for NiTAPc conjugates as reported in this work are for decrease in donor emission. FRET efficiency values determined below are an estimate since there are a wide variety of factors [40, 41] which influences the decrease in QDs emission in addition to FRET.

The FRET efficiencies (*Eff*) were calculated from the quantum yield data using Eq. 3:

$$Eff = 1 - \frac{\Phi_{F(QD)}^{conjugate}}{\Phi_{F(QD)}} \tag{3}$$

where $\Phi_{F(QD)}$ represents the fluorescence quantum yield of the QDs alone and $\Phi_{F(QD)}^{conjugate}$ is fluorescence quantum yield of the conjugates.

$\Phi_{F(QD)}^{conjugate}$ values were calculated according to Eq. 4:

$$\Phi_{F(QD)}^{conjugate} = \Phi_{F(QD)} \frac{F_{QD}^{conjugate}}{F_{QD}} \tag{4}$$

where $\Phi_{F(QD)}$ was used as the standard, $F_{QD}^{conjugate}$ is the fluorescence intensity of the QDs in the conjugated form (QDs-MTAPc) and F_{QD} is the fluorescence intensity of the QD alone. There is substantial decrease in the Φ_F values of the QDs in the conjugates (Table 1), when compared with the value for the QDs alone, due to FRET. The values listed in Table 1 showed that ZnTAPc gave the highest *Eff* value. The *Eff* values are largest where fluorescence quantum yields are lowest as expected. In addition to the concept of FRET, it is noteworthy that the covalent binding of the MPc on the QDs exerts strains on the ligand shell which thus creates new trap states on the QDs surface, leading to decrease in the fluorescence emission [42].

Fluorescence quenching studies were performed to determine the quenching ability of MTAPc on QDs using a mixture of the two as solutions (without a chemical bond). Figure 7 shows the fluorescence emission changes of the QDs in the presence of increasing concentrations of the (OAc)AlTAPc (shown as a representative). It was observed that the fluorescence of the QDs was progressively quenched in the presence of the MTAPcs and as shown in the inset of Fig. 7, a linear plot was observed confirming that Stern-

Table 2 Comparison of the LOD of the proposed nanosensor with some published data for H_2O_2 detection using the QDs-MTAPc nanoprobe. Solvent: 50 mM PBS pH 7.4

QDs Probe	LOD	References
QD_s-AlTAPc	9.8 nM	This work
QD_s-NiTAPc	4.4 nM	This work
QD_s-ZnTAPc	2.2 nM	This work
CdSe@ZnS-Horseradish	284 nM	[47]
MUA-CdSe@ZnS	0.1 mM	[46]
CdTe-Hemoglobin	2,230 nM	[49]

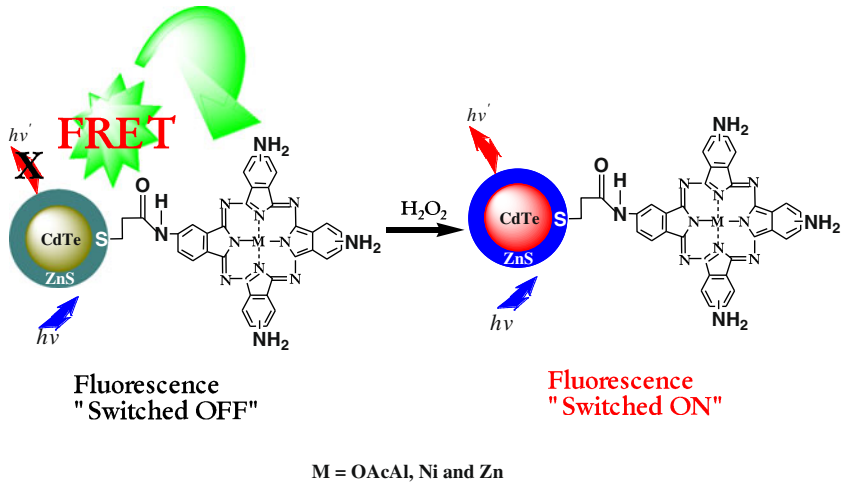

Scheme 2 Schematic representation showing the detection mechanism for H_2O_2 using the QDs-MTAPc nanoprobe

Volmer behaviour was obeyed [43]. There was no shift in the emission spectra of the QDs on interaction with the MTAPc, which implies that the later cannot alter the size and size distribution of the QDs but can only decrease the fluorescence intensity through FRET. The corresponding Stern-Volmer rate constant (K_a) are listed in Table 1 for all the MTAPc complexes. K_a is largest for QDs-NiTAPc but lowest for QDs-AlTAPc, which had the lowest E*ff*.

Hydrogen Peroxide Detection Using CdTe@ZnS-MTAPc

Fluorescence "Switch On" for the Detection of H_2O_2

As discussed above, the covalent binding of the QDs to MTAPc complexes resulted in the fluorescence "switch off" (quenching) of the QDs in the conjugate due to FRET. We explore the possibility of the fluorescence of the linked QDs being "switched on" on interaction with H_2O_2. The presence of different MTAPc covalently linked to the QDs could have a significant influence on the sensitivity of the nanoprobe. Hence, a comparative investigation using, H_2TAPc, (OAc)AlTAPc, NiTAPc and ZnTAPc were carried out. Upon addition of H_2O_2 to QDs-AlTAPc (Fig. 8a), QDs-NiTAPc (Fig. 8b) and QDs-ZnTAPc (Fig. 8c) nanoprobe, the fluorescence of the linked QDs was progressively recovered with the successive increase in H_2O_2 concentration. However, for the QDs-H_2TAPc (Fig. 8d), there was no significant fluorescence enhancement in the presence of varying concentration of H_2O_2. This implies that H_2O_2 does not influence the emission of QDs-H_2TAPc and thus gives a strong indication that the presence of the central metal attached to the MPc, plays a major role in determining the fluorescence property of the QDs-MTAPc on interaction with targeted species. Also, it is generally known that the presence of different central metals ions influences the chemistry of Pcs [44], hence, the varying degree of interactions. It is worth noting that the QDs alone could not detect H_2O_2 with a stable fluorescence signal at the same concentration (of H_2O_2) used for the QDs-MTAPc complexes. Hence, H_2O_2 can only be detected at a much higher

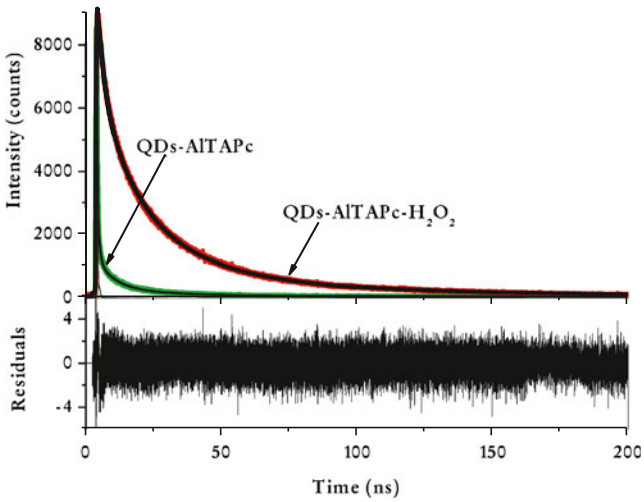

Fig. 9 Overlay of the fluorescence decay curves of QDs-AlTAPc (as a representative) in the absence and presence of 1.6×10^{-8} M H_2O_2

Table 3 Fluorescence lifetimes for a triexponential fit of QDs (alone) and QDs-MTAPc nanoprobe in the absence and presence of H_2O_2 in 50 mM PBS buffer, pH 7.4

Samples	H_2O_2[M]	τ_1 (ns)[a] ±0.1	τ_2 (ns)[a] ±0.1	τ_3 (ns)[a] ±0.02
QDs	0	42.6(0.56)	13.8(0.39)	2.6(0.05)
	1.6×10^{-8}	42.6(0.57)	13.8(0.27)	2.5(0.06)
QDs-AlTAPc	0	24.7(0.57)	8.3(0.27)	1.6(0.06)
	1.6×10^{-8}	46.1(0.61)	8.9(0.27)	2.0(0.02)
QDs-NiTAPc	0	31.2(0.46)	7.9(0.36)	1.6(0.08)
	1.6×10^{-8}	46.9(0.48)	15.2(0.45)	3.0(0.07)
QDs-ZnTAPc	0	31.2(0.54)	6.5(0.38)	0.8(0.08)
	1.6×10^{-8}	42.7(0.59)	13.5(0.36)	2.2(0.05)

[a] Relative abundances in brackets

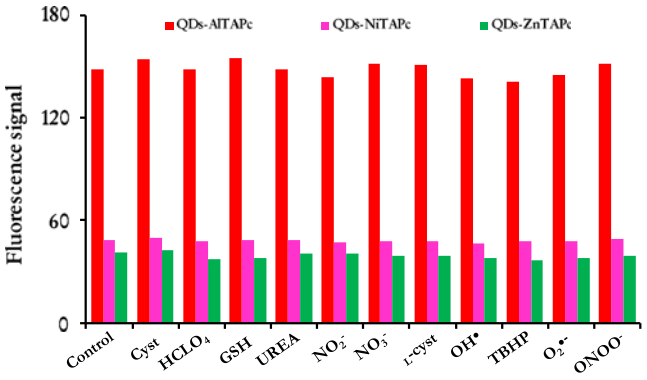

Fig. 10 Effects of different biologically active species on the fluorescence of QDs-MTAPc system. $[H_2O_2]=4.0\times10^{-9}$ M. Other species= 8×10^{-7} M. Control=QDs-MTAPc in the presence of H_2O_2

concentration (plot not shown) by quenching (not enhancement reported here) the fluorescence of the QDs alone as compared to lower concentrations detected by the QDs-MTAPc. Hence, the QDs-MTAPc nanoprobe shows higher sensitivity.

It has been reported that the spacing between the QDs and the quencher (and the concentration of the latter) control the emission enhancement in QDs. Long spaces result in enhancement and short spaces in quenching [45]. We propose that MTAPc acts as a spacer between the QDs and H_2O_2 such that the latter results in enhancement of fluorescence rather than quenching in accordance with literature reports [45].

In order to evaluate the fluorescence enhancement sensitivity of the probe, the fluorescence intensities of the QDs-MTAPc in the absence (F_0) and presence (F) of H_2O_2 was investigated using Eq. 5 [46].

$$\frac{F}{F_0} = 1 + K[H_2O_2] \tag{5}$$

Please note that Eq. 5 relates to F/F_0 (due to enhancement of fluorescence) instead of F_0/F usually employed for quenching of fluorescence. As displayed in the insets of Fig. 8a–c, plots of F/F_0 against H_2O_2 concentrations were linear. Using the value of K in the regression equation as a measure of degree of sensitivity of the nanoprobe, the sensitivity followed the order: QDs-ZnTAPc>QDs-NiTAPc> QDs-AlTAPc (Table 1). The limit of detection (LOD) was evaluated using the equation LOD=3 δ/K, where δ is the standard deviation of blank measurement (n=10) and K is the slope of the calibration graph. Quantitative analysis of this method showed a good LOD for H_2O_2 (Table 2) and followed the order of sensitivity of the nanoprobe. To the best of our knowledge, there are no reports on H_2O_2 detection using QDs-macrocyclic complexes. Hence, we compared our LOD values with other QDs based probe for H_2O_2 [47–49] and results showed our system offered an improvement in the LOD (Table 2).

Proposed Mechanism for the Detection of H_2O_2 (Scheme 2)

We propose that the working principle of the QDs-MTAPc could be elucidated based on the changes in the emission spectra of the linked QDs and time-resolved fluorescence measurements. It is noteworthy that a number of QD-based fluorescent probes have been designed based on the switching "off/on" principle, in which the QDs displays a low/no fluorescence in the unbound state and a recovery of the fluorescence after reaction with (or binding) with an analyte [46, 50–53].

Time resolved fluorescence measurements were carried out. Figure 9 shows the fluorescence decay curve of (OAc)AlTAPc (used as an example) in the absence and presence of a fixed concentration of H_2O_2. As shown in Table 3, the tri-exponential decay lifetimes of the QDs-MTAPc complexes were substantially increased when H_2O_2 was added. When the same equivalent concentration of H_2O_2 was added to the QDs alone, no change in the fluorescence lifetime of the QDs was observed (Table 3).

Table 4 Percentage fluorescence intensity (%FI) change of co-existing biological active species on the detection of 4.0×10^{-9} M H_2O_2 by the proposed QDs-MTAPc nanoprobe. Concentration of interfering ions= 8.0×10^{-7} M. Solvent: 50 mM PBS pH 7.4

Species	QDs-AlTAPc (%FI)	QDs-NiTAPc (%FI)	QDs-ZnTAPc (%FI)
Cysteamine	+3.6	+2.2	+1.8
$HClO_4$	−0.3	−2.1	−10.9
GSH	+4.0	−0.8	−9.2
UREA	−0.1	−0.6	−2.4
NO_2^-	−3.3	−2.6	−2.0
NO_3^-	+1.9	−2.1	−5.0
L-cysteine	+1.4	−2.0	−5.1
OH•	−3.7	−4.8	−8.2
TBHP	−5.1	−1.3	−11.9
$O_2^{\bullet-}$	−2.3	−1.4	−9.4
$ONOO^-$	+1.9	+1.6	+4.8

Based on the data discussed above, the reaction mechanism can be generalised by means of an "off/on" fluorescence principle (Scheme 2) in which the QDs transfers its energy to MTAPc. This then led to a radiationless deactivation of the excited state of the QDs, and the fluorescence is quenched. Upon addition of H_2O_2, the FRET process is interrupted and the fluorescence of the QDs is switched on.

Additionally, since H_2O_2 is a known oxidant, it is also possible that oxidation by MTAPc-H_2O_2 complex switched on the fluorescence of the QDs [54]. Soh et al. [54], have previously shown that oxidation by H_2O_2 switches on the fluorescence of 7-hydroxy-2-oxo-N-(2-(diphenylphosphino) ethyl)-2 H-chromene-3-carboxamide.

Selectivity of the QDs-MTAPc Nanosensor Towards H_2O_2

It is ideal for an efficient fluorescent probe to combine both sensitivity and selectivity for its efficacy. Hence, we investigated (by comparison) the selectivity of the proposed QDs-MTAPc nanosensor towards H_2O_2. It is also noteworthy that since the QDs-MTAPc nanosensor showed excellent sensitivity towards H_2O_2 with varying degree, it is possible that the selectivity of the proposed nanosensor may differ for each QDs-MTAPc conjugate. Therefore, the fluorescence intensity change of a fixed concentration of QDs-MTAPc was studied in the presence of 200-fold excess of co-existing biological active species such as: cysteamine (cys), $HClO_4$, glutathione (GSH), urea, NO_2^-, NO_3^-, L-cysteine (L-cys), hydroxyl radical (OH•), TBHP, superoxide anion ($O_2^{\bullet-}$) and peroxynitrite ($ONOO^-$). A tolerance error of ±5 % in fluorescence intensity (FI) change was taken into consideration. As shown in Fig. 10 (Table 4), the fluorescence response of all co-existing species to the proposed nanosensor varied, depending on the nature of the nanoprobe. Generally, it can be seen from Fig. 10 (Table 4) that even though QDs-ZnTAPc showed excellent sensitivity towards H_2O_2 as previously discussed, it suffered from severe interferences from species like, $HClO_4$, GSH, OH•, TBHP and $O_2^{\bullet-}$. Hence, this probe is not very selective towards H_2O_2. For QDs-AlTAPc, the fluorescence of all co-existing species was rather slight except for TBHP but for QDs-NiTAPc, the effects of all co-existing species were negligible and thus make QDs-NiTAPc the most selective nanoprobe for H_2O_2. Therefore, the order of selectivity of the nanoprobe is: QDs-NiTAPc> QDs-AlTAPc>QDs-ZnTAPc. It is also worth noting that the order of selectivity of the nanoprobe did not follow the same trend with the sensitivity. We have shown in previous reports (by comparative study) [30] that the order of sensitivity of a probe towards ROS may not follow similar trends with its selectivity because steric effects and oxidative shielding of the probe may differ in the presence of co-existing species. DFT calculations showed that there is more electron density on the ring for NiTAPc (0.208), followed by AlTAPc (0.206) and ZnTAPc (0.188). The trend in electron density of the MTAPc was the same with the selectivity trend of the nanoprobe. This may suggest that steric effect and shielding from oxidative attack was more for QDs-NiTAPc than for the other nanoprobe. Since a mutual balance between sensitivity and selectivity need to be achieved for an efficient probe, QDs-NiTAPc shows to be the most effective nanoprobe for H_2O_2.

Conclusions

We have demonstrated in this work that metal phthalocynanine containing amino substituent can be covalently linked to QDs to form a QDs-MTAPc nanoconjugate which can be applied as a luminescence nanosensor for ROS detection with varying degree of sensitivity and selectivity. The nanoconjugates of QDs-AlTAPc, QDs-NiTAPc and QDs-ZnTAPc were characterized by time-resolved fluorescence measurements, TEM, FT-IR and electronic spectroscopy. Experimental results showed that interaction between the QDs and MTAPc occurred through FRET which in turn "switched off" the fluorescence of the QDs. In the presence of varying concentrations of H_2O_2, the fluorescence of the QDs was "switched on" and the degree of sensitivity/LOD followed the order: QDs-ZnTAPc>QDs-NiTAPc>QDs-AlTAPc. The selectivity of the proposed nanosensor followed the order: QDs-NiTAPc>QDs-AlTAPc>QDs-ZnTAPc. We believe this technique will harness a new generation of highly luminescence QDs-MPc nanosensors.

Acknowledgements This work was supported by the Department of Science and Technology (DST) and National Research Foundation (NRF), South Africa through DST/NRF South African Research Chairs Initiative for Professor of Medicinal Chemistry and Nanotechnology as well as Rhodes University and DST/Mintek Nanotechnology Innovation Centre (NIC)—Sensors, South Africa.

References

1. Frasco MF, Chaniotakis N (2009) Semiconductor quantum dots in chemical sensors and biosensors. Sensors 9:7266–7286
2. Wang Y, Chen L (2011) Quantum dots, lighting up the research and development of nanomedicine. Nanomedicine 7:385–402
3. Algar WR, Tavares AJ, Krull UJ (2010) Beyond labels: a review of the application of quantum dots as integrated components of assays, bioprobes, and biosensors utilizing optical transduction. Anal Chim Acta 673:1–25
4. Han C, Haibing L (2010) Host-molecule-coated quantum dots as fluorescent sensors. Anal Bioanal Chem 397:1437–1444
5. Alivisatos AP (2004) The use of nanocrystals in biological detection. Nat Biotechnol 22:47–52
6. Michalet X, Pinaud F, Bentolila LA, Tsay JM, Doose S, Li JJ, Sundaresan G, Wu AM, Gambhir SS, Weiss S (2005) Quantum dots for live cells, in vivo imaging, and diagnostics. Science 307:538–544

7. Medintz IL, Uyeda HT, Goldman ER, Mattoussi H (2005) Quantum dot bioconjugates for imaging, labelling and sensing. Nat Mater 4:435–446
8. Somers RC, Bawendi MG, Nocera DG (2007) CdSe nanocrystal based chem-/bio-sensors. Chem Soc Rev 36:579–591
9. Murphy CJ (2002) Optical sensing with quantum dots. Anal Chem 74:520A–526A
10. Jin T, Fujii F, Yamada E, Nodasaka Y, Kinjo M (2006) Control of the optical properties of quantum dots by surface coating with calix[n]arene carboxylic acids. J Am Chem Soc 128:9288–9289
11. Rakshit S, Vasudevan S (2008) Resonance energy transfer from β-cyclodextrin-capped ZnO:MgO nanocrystals to included Nile red guest molecules in aqueous media. ACS Nano 2:1473–1479
12. Chen C-Y, Cheng C-T, Lai C-W, Wu P-W, Wu K-C, Chou P-T, Chou Y-H, Chiu H-T (2005) Potassium ion recognition by 15-crown-5 functionalized CdSe/ZnS. Chem Commun. doi:10.1039/b512677k
13. Frasco MF, Vamvakaki V, Chaniotakis N (2010) Porphyrin decorated CdSe quantum dots for direct fluorescent sensing of metal ions. J Nanopart Res 12:1449–1458
14. Claessens CG, Hahn U, Torres T (2008) Phthalocyanines: from outstanding electronic properties to emerging applications. Chem Rec 8:75–97
15. Paoletti AM, Pennesi G, Rossi G, Generosi A, Paci B, Albertini VR (2009) Titanium and ruthenium phthalocyanines for NO_2 sensors: a mini-review. Sensors 9:5277–5297
16. D'Souza S, Antunes E, Nyokong T (2011) The interaction between thiol coated CdTe quantum dots and aminophenoxy mono substituted zinc phthalocyanines. Inorg Chim Acta 367:173–181
17. D'Souza S, Antunes E, Litwinski C, Nyokong T (2011) Photophysical effects of zinc monoamino phthalocyanines linked to mercaptopropionic-capped CdTe quantum dots. J Photochem Photobiol A 220:11–19
18. Britton J, Antunes E, Nyokong T (2009) Fluorescence studies of quantum dots and zinc tetraamino phthalocyanine conjugates. Inorg Chem Commun 12:828–831
19. Britton J, Antunes E, Nyokong T (2010) Fluorescence quenching and energy transfer in conjugates of quantum dots with zinc and indium tetraamino phthalocyanines. J Photochem Photobiol A 210:1–7
20. Chidawanyika W, Litwinski C, Antunes E, Nyokong T (2010) Photophysical study of a covalently linked quantum dot–low symmetry phthalocyanine conjugate. J Photochem Photobiol A 212:27–35
21. Khene S, Moeno S, Nyokong T (2011) Voltammetry and electrochemical impedance spectroscopy of gold electrodes modified with CdTe quantum dots and their conjugates with nickel tetraamino phthalocynanine. Polyhedron 30:2162–2170
22. Chen X-L, Li D-H, Yang H-H, Zhu Q-Z, Zheng H, Xu J-G (2001) Study of tetra-substituted amino aluminum phthalocyanine as a new red-region substrate for the fluorometric determination of peroxidase and hydrogen peroxide. Anal Chim Acta 434:51–58
23. Chen X-L, Li D-H, Yang H-H, Zhu Q-Z, Zheng H, Xu J-G (2001) A new red-region substrate, tetra-substituted amino aluminium phthalocyanine, for the fluorimetric determination of H_2O_2 catalyzed by mimetic peroxidises. Analyst 126:523–527
24. Achar BN, Fohlen GM, Parker JA, Keshavayya J (1987) Synthesis and structural studies of metal(II) 4,9,16,23-phthalocyanine tetraamines. Polyhedron 6:1463–1467
25. Frisch MJ, Trucks GW, Schlegel HB, Scuseria GE, Robb MA, Cheeseman JR, Montgomery JA, Vreven JT, Kudin KN, Burant JC, Millam JM, Iyengar SS, Tomasi J, Barone V, Mennucci B, Cossi M, Scalmani G, Rega N, Petersson GA, Nakatsuji H, Hada M, Ehara M, Toyota K, Fukuda R, Hasegawa J, Ishida M, Nakajima T, Honda Y, Kitao O, Nakai H, Klene M, Li X, Knox JE, Hratchian HP, Cross JB, Bakken V, Adamo C, Jaramillo J, Gomperts R, Stratmann RE, Yazyev O, Austin AJ, Cammi R, Pomelli C, Ochterski JW, Ayala PY, Morokuma K, Voth GA, Salvador P, Dannenberg JJ, Zakrzewski VG, Dapprich S, Daniels AD, Strain MC, Farkas O, Malick DK, Rabuck AD, Raghavachari K, Foresman JB, Ortiz JV, Cui Q, Baboul AG, Clifford S, Cioslowski J, Stefanov BB, Liu G, Liashenko A, Piskorz P, Komaromi I, Martin RL, Fox DJ, Keith T, Al-Laham MA, Peng CY, Nanayakkara A, Challacombe M, Gill PMW, Johnson B, Chen W, Wong MW, Gonzalez C, Pople JA (2004) Gaussian 03, Revision E.01. Gaussian, Inc, Wallingford
26. Liu Z, Yin P, Gong H, Li P, Wang X, He Y (2012) Determination of rifampicin based on fluorescence quenching of GSH capped CdTe/ZnS QDs. J Lumin 132:2484–2488
27. Algar WR, Krull UJ (2006) Adsorption and hybridization of oligonucleotides on mercaptoacetic acid-capped CdSe/ZnS quantum dots and quantum dotoligonucleotide conjugates. Langmuir 22:11346–11352
28. Liu Y, Yu J (2010) In situ synthesis of highly luminescent glutathione-capped CdTe/ZnS quantum dots with biocompatibility. J Colloid Interface Sci 351:1–9
29. Talapin DV, Mekis I, Götzinger S, Kornowski A, Benson O, Weller H (2004) CdSe/CdS/ZnS and CdSe/ZnSe/ZnS core-Shell-Shell nanocrystals. J Phys Chem B 108:18826–18831
30. Adegoke O, Nyokong T (2012) A comparative study on the sensitive detection of hydroxyl radical using thiol-capped CdTe and CdTe/ZnS quantum dots. J Fluoresc 22:1513–1519
31. Adegoke O, Nyokong T (2012) Probing the sensitive and selective luminescent detection of peroxynitrite using thiol-capped CdTe and CdTe@ZnS quantum dots. J Lumin 134:448–455
32. Grabolle M, Spieles M, Lesnyak V, Gaponik N, Eychmüller, Resch-Genger U (2009) Determination of the fluorescence quantum yield of quantum dots: suitable procedures and achievable uncertainties. Anal Chem 81:6285–6294
33. Xia X, Liu Z, Du G, Li Y, Ma M, Yao K (2012) Blue–green luminescent CdZnSeS nanocrystals synthesized with activated alkyl thiol. J Lumin 132:100–105
34. Masilela N, Nyokong T (2012) The photophysical and energy transfer behaviour of low symmetry phthalocyanine complexes conjugated to coreshell quantum dots: an energy transfer study. J Photochem Photobiol A 247:82–92
35. Yan C, Tang F, Li L, Li H, Huang X, Chen D, Meng X, Ren J (2010) Synthesis of aqueous CdTe/CdS/ZnS core/shell/shell quantum dots by a chemical aerosol flow method. Nanoscale Res Lett 5:189–194
36. Jenkins R, Synder RL (1996) Introduction to X-ray diffractometry. Wiley, New York
37. Mohan T, Kargl R, Köstler S, Doliška A, Findenig G, Ribitsch V, Stana-Kleinschek K (2012) Functional polysaccharide conjugates for the preparation of microarrays. Appl Mater Interfaces 4:2743–2751
38. Ghosh S, Saha A (2009) Synthesis and spectral studies of CdTe–dendrimer conjugates. Nanoscale Res Lett 4:937–941
39. Yun C, Javier SA, Jennings T, Fisher M, Hira S, Peterson S, Hopkins B, Reich NO, Strouse GF (2005) Nanometal surface energy transfer in optical rulers, breaking the FRET barrier. J Am Chem Soc 127:3115–3119
40. Takanishi CL, Bykova EA, Cheng W, Zheng J (2006) Quantification of GFP-based FRET in live cells. Brain Res 1091:132–139
41. Blaudeck T, Zenkevich EI, Cichos F, von Borczyskowski C (2008) Probing wave functions at semiconductor quantum-dot surfaces by non-FRET photoluminescence quenching. J Phys Chem C 112:20251–20257
42. Zenkevich EI, Stupak AP, Kowerko D, von Borczyskowski C (2012) Influence of single dye molecules on temperature and time dependent optical properties of CdSe/ZnS quantum dots: ensemble and single nanoassembly detection. Chem Phys 406:21–29
43. Van de Weert M, Stella L (2011) Fluorescence quenching and ligand binding: a critical discussion of a popular methodology. J Mol Struct 998:144–150

44. Wang A, Long L, Zhang C (2011) Synthesis and properties of photo-activable phthalocyanines: a brief overview. J Incl Phenom Macrocycl Chem 71:1–24
45. Chandra S, Doran J, McCormack SJ, Kennedy M, Chatten AJ (2012) Enhanced quantum dot emission for luminescent solar concentrators using plasminic interaction. Sol Energ Mat Sol C 98:385–390
46. Wang S, Han M-Y, Huang D (2009) Nitric oxide switches on the photoluminescence of molecularly engineered quantum dots. J Am Chem Soc 131:11692–11694
47. Wang Z, Xu Q, Wang H-Q, Yang Q, Yu J-H, Zhao Y-D (2009) Hydrogen peroxide biosensor based on direct electron transfer of horseradish peroxidase with vapor deposited quantum dots. Sens Actuators B 138:278–282
48. Gill R, Bahshi L, Freeman R, Willner I (2008) Optical detection of glucose and acetylcholine esterase inhibitors by H_2O_2-sensitive CdSe/ZnS quantum dots. Angew Chem Int Ed 47:1676–1679
49. Xu Q, Wang J-H, Wang Z, Wang H-Q, Yang Q, Zhao Y-D (2009) Biosensor for hydrogen peroxide based on chitosan and nanoparticle complex film—modified glassy-carbon electrodes. Anal Lett 42:2496–2508
50. Algarra M, Campos BB, Aguiar FR, Rodriguez-Borges JE, Esteves da Silva JCG (2012) Novel β-cyclodextrin modified CdTe quantum dots as fluorescence nanosensor for acetylsalicylic acid and metabolites. Mater Sci Eng C 32:799–803
51. Li H, Qu F (2007) Selective inclusion of polycyclic aromatic hydrocarbons (PAHs) on calixarene coated silica nanospheres englobed with CdTe nanocrystals. J Mater Chem 17:3536–3544
52. Xu H, Miao R, Fang Z, Zhong X (2011) Quantum dot-based "turn-on" fluorescent probe for detection of zinc and cadmium ions in aqueous media. Anal Chim Acta 687:82–88
53. Rueda-Rama MJ, Hall EAH (2008) Multiplexed energy transfer mechanisms in a dual-function quantum dot for zinc and manganese. Analyst 134:159–169
54. Soh N, Sakawaki O, Makihara K, Odo Y, Fukaminato T, Kawai T, Irie M, Imato T (2005) Design and development of a fluorescent probe for monitoring hydrogen peroxide using photoinduced electron transfer. Bioorg Med Chem 13:1131–1139